ADVANCED ELECTRONIC MATERIALS
www.advelectronicmat.de

On Charge Carrier Density in Organic Solar Cells Obtained via Capacitance Spectroscopy

Joachim Vollbrecht and Viktor V. Brus**

The determination of the voltage-dependent density of free charge carriers via capacitance spectroscopy is considered an important step in the analysis of emerging photovoltaic technologies, such as organic and perovskite solar cells. In particular, an intimate knowledge of the density of free charge carriers is required for the determination of crucial parameters such as the effective mobility, charge carrier lifetime, nongeminate recombination coefficients, average extraction times, and competition factors. Hence, it is paramount to verify the validity of the commonly employed approaches to obtain the density of free charge carriers. The advantages, drawbacks, and limitations of the most common approaches are investigated in detail and strategies to mitigate misleading values are explored. To this end, two types of nonfullerene organic solar cells based on a PTB7-Th:ITIC-2F blend and a PM6:Y6 blend, respectively, are used as a case study to assess how subsequent analyses of the nongeminate recombination dynamics depend on the chosen approach to calculate the density of free charge carriers via capacitance spectroscopy.

1. Introduction

In the recent years, new alternatives to classical inorganic semiconductors have garnered a lot of attention. A plethora of applications have been reported based on organic and organic–inorganic hybrid semiconductors, among others light emitting diodes,[1,2] field effect transistors,[3–5] solar cells,[6,7] energy harvesting devices,[8] photodiodes,[9,10] sensors, and wearable electronics.[11] For the continued improvement of these materials and the devices based on them an important first step is to obtain the density of free charge carriers n, also commonly known as charge carrier density. Specifically in the case of solar cells, an intimate knowledge of the charge carrier density n allows—in combination with more classical measurement techniques such as current density-voltage (J–V) curves—the quantification of crucial parameters related to the nongeminate recombination and extraction dynamics. However, only integral parameters, e.g., electrical conductivity, impedance, open-circuit voltage, etc., can be measured directly by experiments. The primary challenge in more advanced analyses lies therefore in finding the appropriate relationship between the measured integral parameters and the charge carrier density. Most common techniques used to study charge recombination do not require the calculation of the charge carrier density, but are only of a qualitative nature unable to yield quantitative figures of merit such as the charge carrier lifetime τ_{rec} or the recombination coefficient k_{rec}.[12,13] In addition, more advanced techniques with which one can obtain quantitative results usually are not performed on real devices under operating conditions or do not take the voltage dependence of the recombination into account.[14–16] Therefore, more in-depth analyses developed and refined over the recent years based on a variant of impedance spectroscopy, namely capacitance spectroscopy, have started to find more frequent application. In part, this is due to the fact that quantitative results for organic solar cells under operating conditions are accessible, allowing to determine the charge carrier density n—and by extension parameters such as recombination coefficients k_{rec} or average extraction times τ_{ex}.[17–20] All of the various analyses reported strongly rely on an accurate determination of the charge carrier density n via capacitance spectroscopy. However, several different approaches to obtain the charge carrier density have been described in the literature. Hence, a systematic comparison of these different approaches and a detailed assessment of their individual advantages, drawbacks and limitations are required to enable researchers to choose the appropriate strategy to analyze their results.

2. Results and Discussion

The different approaches that will be compared and discussed in more detail below require capacitance measurements of the solar cells in the dark and under illumination (100 mW cm^{-2} AM1.5G) at applied DC biases relevant to the operation of solar cells ($V_{DC} \approx -3$ to $+1$ V). In particular, reliable capacitance values

Dr. J. Vollbrecht
Soft Matter Physics Group, Institute of Physics and Astronomy
University of Potsdam
Potsdam-Golm 14476, Germany
E-mail: vollbrecht@uni-potsdam.de

Prof. V. V. Brus
Department of Physics, School of Sciences and Humanities
Nazarbayev University
Nur-Sultan 010000, Republic of Kazakhstan
E-mail: vvbrus@gmail.com

The ORCID identification number(s) for the author(s) of this article can be found under https://doi.org/10.1002/aelm.202000517.

DOI: 10.1002/aelm.202000517

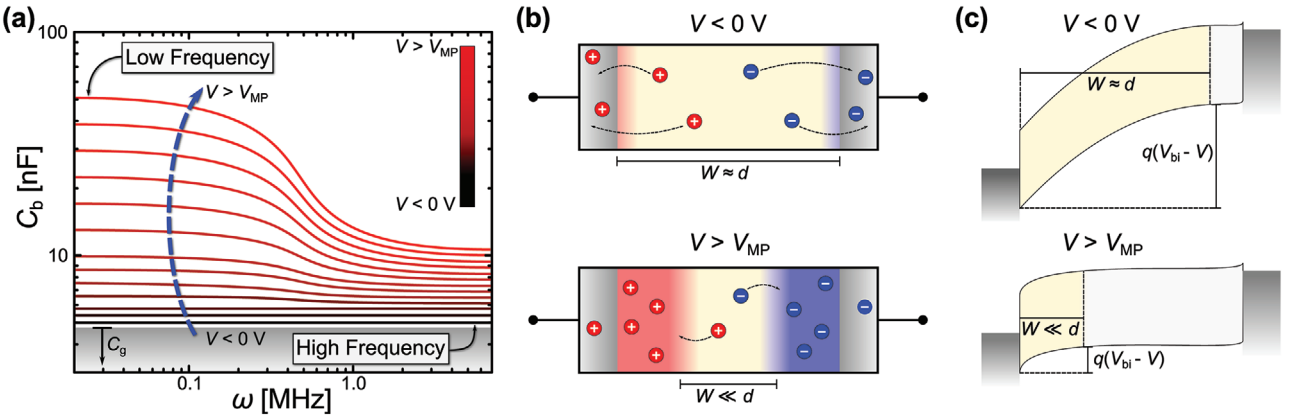

Figure 1. a) General frequency dependence of the corrected capacitance C_b at different applied biases V of organic solar cells. b) Idealized charge distribution and variable, and voltage-dependent depletion width W in the active layer under the assumption of an intrinsic semiconductor. c) Energy levels, band bending, and variable depletion width W in the active layer under the assumption of a doped semiconductor.

are necessary over a wide frequency range that also includes the low-frequency (LF) plateau and saturated high-frequency (HF) regime (cf. **Figure 1**a). The investigation of organic solar cells employing a blend of PTB7-Th:ITIC-2F has yielded capacitance values that fulfill the requirements for this comparative investigation, although the tested devices might exhibit moderate power conversion efficiencies (PCE = 8.6%) by today's standards (cf. Figures S1 and S2a, Supporting Information).[18] In addition, high performing solar cells (PCE = 14.6%) based on the blend PM6:Y6 have also been studied via capacitance spectroscopy, although the saturated high-frequency regime was not easily resolved (cf. Figure S2b, Supporting Information).[19] The datasets already published in refs. [18,19] will be used for this comparison. All relevant parameters for the analyses and calculations described below are listed in Table S1 (Supporting Information), and the *J*–*V* curves of the two studied blend systems are shown in Figure S1 in the Supporting Information.

2.1. Measurement of the Capacitance in the Bulk-Heterojunction

As mentioned above, capacitance spectroscopy is a variant of impedance spectroscopy and the reader is referred to the following previous studies that give an excellent introduction to the general topic of impedance spectroscopy in the scope of organic solar cells.[21,22]

Before any meaningful analysis can start, it is necessary to take into account contributions to the measured capacitances that are not related to the active layer. Two corrections have to be made, namely, adjustments due to the influence of the series resistance and due to parasitic inductance of the connections to the solar cell, to obtain the capacitance of the bulk-heterojunction C_b[23]

$$C_b = -\frac{1}{\omega}\left[\frac{Z'' - \omega L_{ind}}{(Z' - R_{series})^2 + (Z'' - \omega L_{ind})^2}\right] \quad (1)$$

where ω is the angular frequency of the AC component of the bias, Z' and Z'' are the real and imaginary components of the measured impedance, L_{ind} is the parasitic inductance of the connected wires, and R_{series} is the series resistance of the solar cell. These corrections are important specifically at higher frequencies as the contributions from the parasitic inductance start to dominate the measured capacitance.[20] This behavior also poses a significant challenge for the investigation of high performing solar cells, since these devices exhibit the saturated HF regime beyond the ω = 10 MHz threshold. In such a frequency range, the influence of the parasitic inductance overwhelms the signal from the active layer and efforts to correct the measured capacitance become increasingly less reliable. The first effects of this phenomenon can be seen in the HF regime of the chosen dataset for the PM6:Y6 solar cell (Figure S2, Supporting Information).[19]

In addition to the corrections of the capacitance, it is also required to take precautions against the voltage loss over the series resistance, specifically if results from the capacitance measurements are put in relation to results obtained from *J*–*V* characteristics. The corrected voltage can be expressed by

$$V_{cor} = V - J \cdot R_{series} \quad (2)$$

where V_{cor} is the corrected voltage, J is the current density, and where R_{series} is the series resistance, which is equal to the saturated differential resistance at forward bias obtained from the *J*–*V* curve (i.e., $\partial V/\partial J$ = const.).[24]

One of the first results available from the C_b–ω curves is the geometric capacitance C_g, which is the capacitance caused by the electrodes forming a plate capacitor. When trying to determine C_g, contributions due to injected and/or photogenerated charge carriers should be minimal, which means that C_g should be frequency independent and available from the C_b measurements at large reverse biases (V_{DC} = −3 V) in the dark

$$C_b^{dark}(-3\,V) = C_g = \frac{\varepsilon_r \varepsilon_0 A}{L} \quad (3)$$

where ε_0 is the vacuum permittivity, ε_r is the relative dielectric constant of the layers between the electrodes, L is the distance between the electrodes and therefore equals to the active layer thickness, and A is the area of the electrodes.[18] A rearranged version of Equation (3) has been used in the literature to determine the relative dielectric constants ε_r of blend

systems in bulk-heterojunctions.[25] As will be discussed later in the manuscript, it is also important to choose the correct frequency range to determine the exact value of C_g, since the capacitance C_b—even at large reverse biases—is not completely independent of the frequency ω.

2.2. Determination of the Charge Carrier Density

All approaches to determine the charge carrier density based on capacitance spectroscopy rely on the assumption that the free charge carriers present in the active layer, either due to injection and/or photogeneration, cause a certain capacitance, often called internal or chemical capacitance C_{chem}. The integration of this chemical capacitance C_{chem} over the voltage is then assumed to comprise the voltage-dependent part of the total charge carrier density, which in this study shall be called excess charge carrier density n_{exc}. At this point the DC bias V will have to be converted to the corrected voltage V_{cor}, as described in Equation (2), since the integration over V would result in an overestimated charge carrier density n. The second term necessary to obtain the total charge carrier density is the voltage-independent saturated charge carrier density n_{sat}. The following relationship can then be employed

$$n = n_{sat} + n_{exc} = \underbrace{\frac{1}{qAL} C_{sat}\left(V_0 - V_{sat}\right)}_{\text{saturated charge carrier density}} + \underbrace{\frac{1}{qAL}\int_{V_{sat}}^{V_0} C_{chem}\,\mathrm{d}V_{cor}}_{\text{excess charge carrier density}} \quad (4)$$

where A is the area of the solar cell, L is the thickness, q is the elementary charge, V_{sat} is the reverse bias at which the photocurrent density J_{ph} saturates, V_0 is the forward bias at which the photocurrent density is equal to zero ($J_{ph} = 0$), and where C_{sat} is the capacitance caused by the charge carriers n_{sat}; the definition of C_{sat} will be discussed later in detail. So far, in most cases the analyses stemming from capacitance spectroscopy related the charge carrier density n to the photocurrent density J_{ph} of the tested solar cells. However, an argument can be made that the recombination dynamics of a solar cell also equally involve injected charge carriers, which would mean that not the photocurrent density J_{ph} but rather the total current density J needs to be considered. Under open-circuit conditions the current in the external circuit is equal to zero. This situation can be interpreted in several ways. In the first case, all injected charge carriers recombine with the photogenerated charge carriers inside the device. In the second case, only a part of the injected charge carriers passes through the active layer and forms some injected current which is compensated by the residual photocurrent causing the net total current in the external circuit to be zero. Therefore, the recombination current density will lie between these two values ($J_{ph} \leq J_{rec} \leq J$).

In addition, a study using impedance spectroscopy published by Boix et al. in 2011 showed conclusively for P3HT:PCBM blends that under open-circuit conditions the photogenerated current is canceled by the recombination current in a kinetic balance, which further allowed to establish a relationship between the recombination current under open-circuit and photocurrent at short-circuit conditions.[26]

In this study, we will focus on analyses employing J_{ph} in favor of brevity, but the aforementioned points should nonetheless be considered.

The need for n_{sat} stems from the fact that even under high reverse bias a certain part of the photogenerated charge carriers cannot be extracted and remains in the active layer. As described by Proctor et al. in ref. [17], the lower boundary of the integral could start from any voltage V_X as long as $n(V_X)$ is also known. To clarify, in this context the index X is not a variable describing a position within the active layer, but merely acts as a placeholder. Usually, V_{sat} is chosen as a starting point since the generation rate should be constant and nongeminate recombination should be negligible in the bias regime where the photocurrent density J_{ph} saturates, which is typically at $V_{sat} = -0.$ to -3.0 V.[17] As depicted in Equation (4), the sum of the saturated charge carrier density n_{sat} and the excess charge carrier density n_{exc}—i.e., the integral of C_{chem}—then yields the total charge carrier density n of the tested solar cell, which is the modus operandi common for all approaches—with the exception of method (VI)—that will be discussed below. The distinctions between the approaches arise from the different definitions of the chemical capacitance C_{chem} and the saturation capacitance C_{sat}.

2.2.1. Chemical Capacitance and Excess Charge Carrier Density

First, let us take a detailed look at the different approaches to calculate the chemical capacitance C_{chem}. In the first or classical approach—as described by Garcia-Belmonte et al. in ref. [27]—C_{chem} can be thought of as the difference between the capacitance C_b in the LF range measured under illumination and the capacitance C_b at large reverse bias—i.e., the saturation voltage V_{sat}—under the same illumination

$$C_{chem} = C_{b(LF)}\left(V_{cor}\right) - C_{b(LF)}\left(V_{sat}\right) \quad (5)$$

Note that in both datasets chosen for this comparison $V_{sat} = -3$ V and that under illumination refers to 1 Sun (100 mW cm^{-2} AM1.5G). In principle, C_{chem} can be determined this way also for measurements in the dark, however with the limitation that $C_{sat} \to 0$, as we will discuss later. The assumption for this classical approach is that any increase of the capacitance $C_b(V_{cor})$ compared to $C_b(V_{sat})$ has to be caused by free charge carriers in the active layer. However, as pointed out by Brus et al. in ref. [20] the definition of C_{chem} shown in Equation (5) does not take into account the capacitance C_M, which is the voltage-dependent Maxwell displacement current capacitance of the depletion region.[20,28] The changes of the depletion width W can be described for the case of an intrinsic semiconductor, where voltages approaching open-circuit conditions would result in a depletion width smaller than the thickness of the active layer ($W \ll d$). This scenario can be described by an idealized capacitor with parallel plates with its "electrodes" lying within the active layer due to the diffusion of electrons and holes from the respective electrodes inside the active layer.[29,30] Similarly, a doped semiconductor would exhibit a similar behavior due to changes in the band bending, and thus changes of the thickness of the depletion

layer (cf. Figure 1b,c). A mix of these two cases can be expected in the case of bulk-heterojunctions.

Therefore, neglecting the influence of C_M would result in an overestimation of C_{chem} and ultimately the charge carrier density n. The relationship between C_b and C_{chem} has to be expanded as follows

$$C_b = \frac{C_{chem}}{\left(1+\left[\omega\tau_{IS}\right]^2\right)^{0.5+\delta}} + C_M \tag{6}$$

where ω is the angular frequency of the AC bias, τ_{IS} is the time constant which determines the response of the free charge carriers to the AC bias and should not be mistaken for the charge carrier lifetime τ_{rec}, and δ is an empirical parameter. Bulk-heterojunctions typically exhibit values for δ between two cases ($0.5 \leq \delta \leq 2$).[20] Under open-circuit conditions, Equation (6) can be used to fit the measured values of the corrected capacitance C_b. This can be a useful verification of the corrected capacitance C_b, especially if τ_{rec} can be determined via an independent measurement, since the time constant τ_{IS} is related to the charge carrier lifetime τ_{rec} (cf. Figures S2b and S2d, and Equations (S1)–(S6), Supporting Information). In the case of the PM6:Y6 solar cells, it can be concluded that the HF regime is indeed reasonably well resolved, since the fit of C_b results in a charge carrier lifetime τ_{rec} comparable to the values determined via an independent measurement (cf. Table S2, Supporting Information).

The frequency dependence of Equation (6) may result in three distinct frequency regimes (low-, mid-, and high-frequency), but as pointed out earlier, the two important regimes for this analysis are the LF and HF ranges. In the LF regime ($\omega\tau \ll 1$) Equation (6) can be simplified to

$$C_{b(LF)} = C_{chem} + C_M \tag{7}$$

and in the HF regime ($\omega\tau \gg 1$) it is assumed that the free charge carriers are not able to follow the AC signal, which results in $C_{chem} \rightarrow 0$ and therefore $C_{b(HF)} = C_M$. By rearranging Equation (7) and inserting the expression for C_M in the HF regime depicted previously, it is possible to determine the chemical capacitance C_{chem}, while also correcting for the contributions of the voltage-dependent Maxwell displacement capacitance C_M

$$C_{chem} = C_{b(LF)} - C_{b(HF)} \tag{8}$$

This frequency differential (FD) approach is therefore experimentally accessible, if the saturation of C_b in the HF regime can be resolved, which is not always the case as mentioned earlier.

A third approach was introduced by Zonno et al. in ref. [31], where the effect of free charge carriers within the active layer on the electric field was considered. This aspect then causes a nonlinear electrode charge in contrast to the linear geometric capacitance C_g that is often employed, most specifically when using the classical approach introduced by Garcia-Belmonte discussed at the beginning of this section. However, the determination of this nonlinear behavior is not straight forward and cannot easily be accessed experimentally. Hence, Zonno et al. suggested instead taking the relative photogenerated excess charge carrier density into account for the calculation of C_{chem}, which in essence is the difference between the LF capacitance under illumination relative to the capacitance in the dark at the same applied bias and frequency

$$C_{chem} = C^{1sun}_{b(LF)} - C^{dark}_{b(LF)} \tag{9}$$

This photogenerated excess (PE) approach was investigated by Zonno et al. using SCAPS simulations of an intrinsic solar cell and experimental data of a PTB7-Th:$PC_{71}BM$ solar cell.[31] This approach also relates best to the photocurrent density J_{ph}, as it takes the difference between measurements of the capacitance under illumination and in the dark.

The classical, FD, and PE approaches to determine C_{chem} for the PTB7-Th:ITIC-2F devices are summarized and compared in **Figure 2**, whereas the corresponding plots of the PM6:Y6 devices are displayed in, cf., Figure S3 in the Supporting Information. The colored areas in the C_b–V_{cor} plot (Figure 2a; Figure S3a, Supporting Information) correlate directly to the excess—i.e., voltage dependent—part of the charge carrier density and therefore visualize the integral in Equation (4).

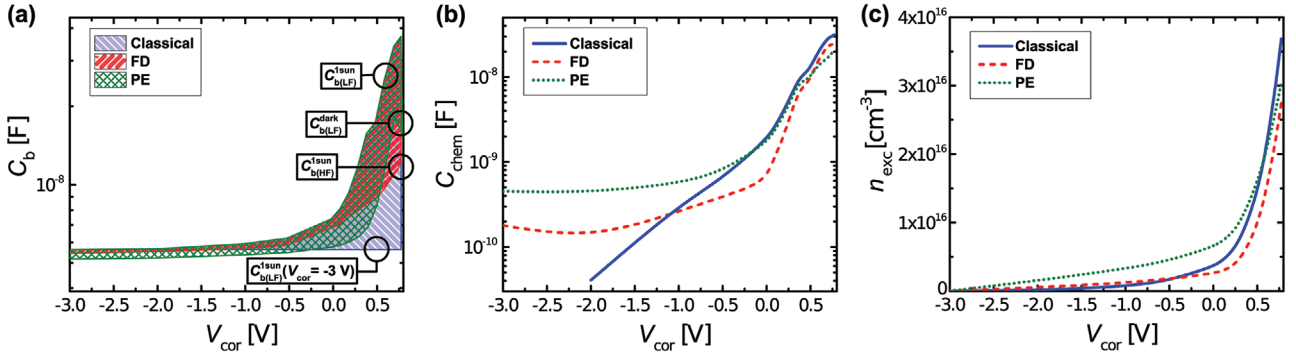

Figure 2. a) Corrected capacitance C_b of the PTB7-Th:ITIC-2F devices under illumination and in the dark. The different colored areas correlate to the different excess charge carrier densities n_{exc}. b) Chemical capacitance C_{chem} determined via the classical, frequency differential (FD), and photogenerated excess (PE) approaches. It should be noted that for the classical approach $C_{chem}(-3\ V) = 0$, which cannot be represented in the semilogarithmic plot. c) Direct comparison of the excess charge carrier densities n_{exc} of the three different approaches. The corresponding plots for the PM6:Y6 device can be found in, cf., Figure S3 in the Supporting Information.

In direct comparison, it can be seen that in both cases the classical approach yields the lowest excess charge carrier density n_{exc} at reverse bias while at the same time exhibiting the highest n_{exc} at high forward bias (cf. Figure 2; Figure S3, Supporting Information), which is not surprising as it will generally overestimate the capacitance at forward biases due to the lack of corrections for the varying depletion width. Interestingly, there seem to be similar trends between the studied solar cells when comparing the FD and PE approaches. For both devices, the n_{exc} obtained via the FD approach is smaller than the value obtained via the PE approach.

2.2.2. Saturated Capacitance and Charge Carrier Density

As described by Equation (4), the determination of the excess charge carrier density n_{exc}—i.e., the integral—is only one of the two terms required for the calculation of the total charge carrier density n, the yet not discussed term being the saturated charge carrier density n_{sat}. In most studies, the classical approach to calculate n_{sat} has been by a method described by Proctor et al. in ref. [17] where the assumption is that the saturated capacitance C_{sat} is the difference between the LF capacitance under illumination at V_{sat} compared to the geometric capacitance C_g. According to the literature, the geometric capacitance C_g is defined as the LF capacitance at V_{sat} of the solar cell in the dark. These assumptions yield

$$C_{sat} = C^{1sun}_{b(LF)}(V_{sat}) - C^{dark}_{b(LF)}(V_{sat}) = C^{1sun}_{b(LF)}(V_{sat}) - C_{g(LF)} \quad (10)$$

Similar to Figure 2a, it is possible to visualize the product of C_{sat} and the voltage range (V_0–V_{sat}) in a C_b–V_{cor} plot (PTB7-Th:ITIC-2F: **Figure 3**a; PM6:Y6: Figure S4a, Supporting Information).

Specifically when the classical approach for the excess charge carrier density n_{exc} is combined with the classical approach for the calculation of the saturated charge carrier density n_{sat}, it can be seen that the entire area below the LF capacitance C_b under illumination and at different biases contributes to the total charge carrier density n, assuming that the geometric capacitance C_g is subtracted beforehand. This can be observed for both tested devices, although the contribution of n_{sat} to the overall charge carrier density n is very small in the case of the high performing PM6:Y6 solar cells. While these results conceptually make sense in the framework of the classical approach, using this method of determining the saturated charge carrier density n_{sat} in combination with either the FD or PE approach for calculating n_{exc} will result in overestimated total charge carrier densities n.

To facilitate the discussion of the different approaches addressed within this study, an overview of the relevant combinations of n_{exc} and n_{sat} is displayed in **Figure 4**. These relevant approaches will now be described by their respective roman number.

Combinations of the FD or PE approach to obtain n_{exc} with the classical method to determine n_{sat}, i.e., approach (II) or (III) in Figure 4, have been frequently used in the literature without—to the best of our knowledge—ever addressing the potential of overestimations.[18,20,31] These overestimations are visualized in Figure 3b and Figure S4b (Supporting Information), where the area representing the product of C_{sat} and (V_0–V_{sat}) in the C_b–V_{cor} plot is magnified and the areas depicting the excess charge carrier densities n_{exc} obtained from the classical, FD, and PE approach are overlaid. Where there is a seamless transition from the area related to the classical n_{sat} to the area related to n_{exc} determined via the classical approach, there are overlaps—specifically at reverse bias—between the classical n_{sat} area and the n_{exc} areas obtained from the FD and PE approach. In essence, this means that during the calculation of the total charge carrier density n, the overlapping areas are "counted twice," ultimately leading to overestimations, specifically at reverse bias. In the case of the PTB7-Th:ITIC-2F solar cells, for the FD approach 9.19% of the classical n_{sat} area overlaps with the area related to n_{exc}, whereas 49.22% of the classical n_{sat} area overlaps with the area related to n_{exc} when employing the PE approach. For the PM6:Y6 devices, overestimations of 48.22% and 31.26% can be observed, respectively (cf. Figure S4b, Supporting Information). The easiest course of action would be to simply correct the classically determined n_{sat} by subtracting the overlapping area, therefore making sure that there is no charge carrier density counted twice. Instead, we opt to mitigate these overestimations by reassessing the definition of C_{sat} altogether and adapt them to the specific method used to calculate n_{exc}. For the FD approach, the first correction would be to replace

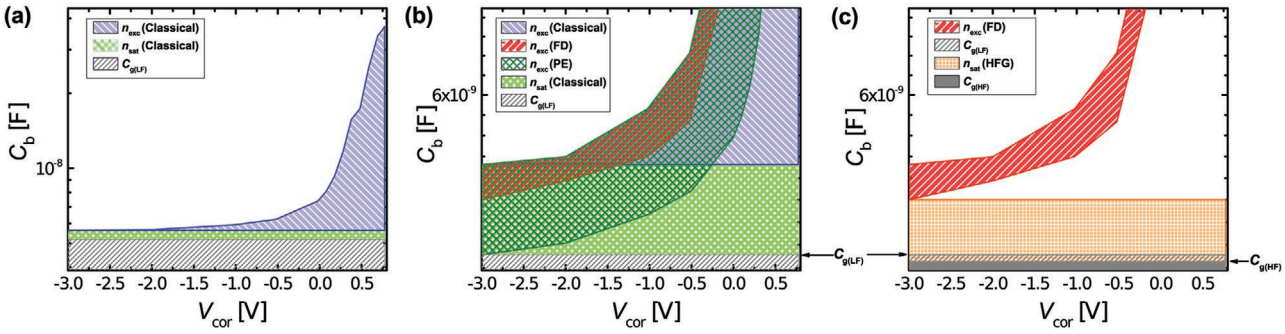

Figure 3. Corrected capacitance C_b at different biases; the areas visualize the excess charge carrier densities n_{exc}—i.e., the integrals of the chemical capacitance C_{chem}—of the classical, FD, and PE approaches as well as the saturated charge carrier density n_{sat} and geometric capacitance C_g obtained via the classical and HFG methods, respectively. The corresponding plots for the PM6:Y6 device can be found in, cf., Figure S4 in the Supporting Information.

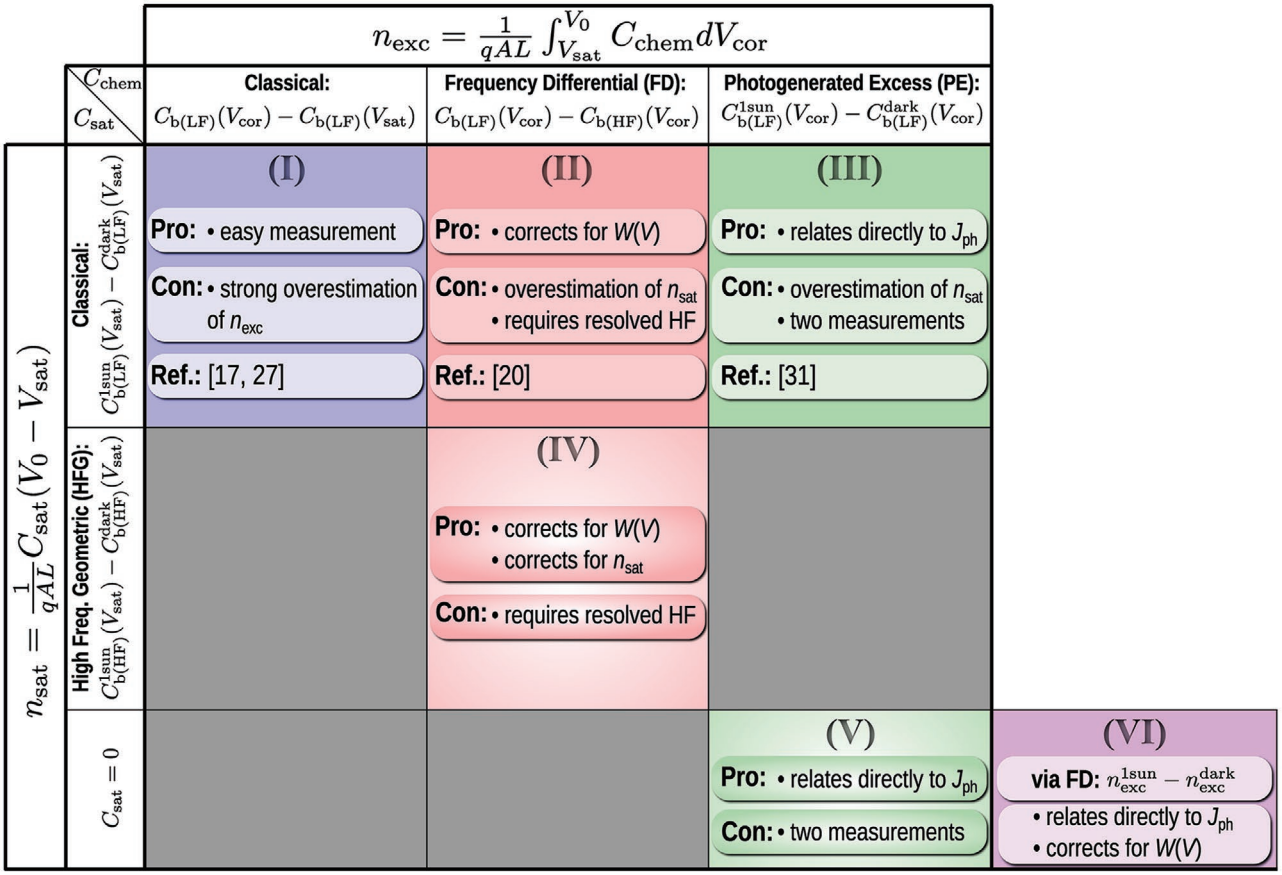

Figure 4. Matrix overview of the different approaches to determine the total charge carrier density n by using appropriate combinations of the excess and saturated charge carrier densities n_{exc} and n_{sat}, respectively. The six relevant approaches are highlighted and are subsequently described by their respective roman numbers. Parts of the matrix with a gray background were not considered, as they do not constitute meaningful combinations of n_{exc} and n_{sat}.

the minuend in Equation (10)—i.e., $C_{\mathrm{b(LF)}}(V_{\mathrm{sat}})$ under illumination—by the lowest capacitance at V_{sat} involved so as to remove any overlaps. In case of the FD approach, $C_{\mathrm{b(HF)}}(V_{\mathrm{sat}})$ under illumination would be used. Additionally, the correct value for C_{g} is equal to the capacitance measured in the dark at high reverse bias in the HF regime rather than the LF regime ($C_{\mathrm{b(HF)}}(V_{\mathrm{sat}})$ vs $C_{\mathrm{b(LF)}}(V_{\mathrm{sat}})$, respectively). This can be rationalized by the still present frequency dependence of $C_{\mathrm{b}}(V_{\mathrm{sat}})$ in the dark, even though this dependence might be very small. This frequency dependence is most likely the result of parasitic effects either from free charges or from traps. For the cases studied here, the correctly determined value of C_{g} will be slightly smaller than $C_{\mathrm{b(LF)}}(V_{\mathrm{sat}})$ in the dark. The changes due to these corrections are visualized in Figure 3c and Figure S4c (Supporting Information); this new method is summarized in Figure 4 under (IV). The difference between approaches (II) and (IV) are miniscule in the case of the PM6:Y6 solar cell, since n_{sat} plays such a minor role in comparison to the excess charge carrier density n_{exc} to begin with. In contrast, the PTB7-Th:ITIC-2F solar cells exhibit a more pronounced difference between (II) and (IV) since in this case n_{sat} is more important with regard to the total charge carrier density n. More advanced calculations for n_{sat} have been proposed by Heiber et al. that also take into account field-dependent charge generation and mobilities, however, they are beyond the scope of this study since they require iterative calculations and are therefore only mentioned here for completeness.[14]

In the case of the PE approach, the question should be posed whether there actually exists the need for $C_{\mathrm{sat}} > 0$. Any photogenerated charge carrier that is not able to reach the electrodes should be accounted for by taking the difference between the capacitance under illumination, which results from photogenerated and injected charge carriers, and the capacitance in the dark, which results only from injected charge carriers, any parasitic effects due to traps notwithstanding. Therefore, the appropriate correction for the PE approach would be to simply neglect n_{sat}; this method is summarized in Figure 4 under (V).

Furthermore, a sixth approach (VI) can be introduced, which corrects for the voltage-dependent depletion width W and which relates to the photocurrent density J_{ph}, therefore taking aspects of the FD and PE approaches, though it does not fit into the matrix overview shown in Figure 4. In particular, the FD method is used to determine the excess charge carrier density n_{exc} for the illuminated device and the device in the dark, and then the difference between these two values is taken to yield the charge carrier density n; no saturated charge carrier density n_{sat} is required.

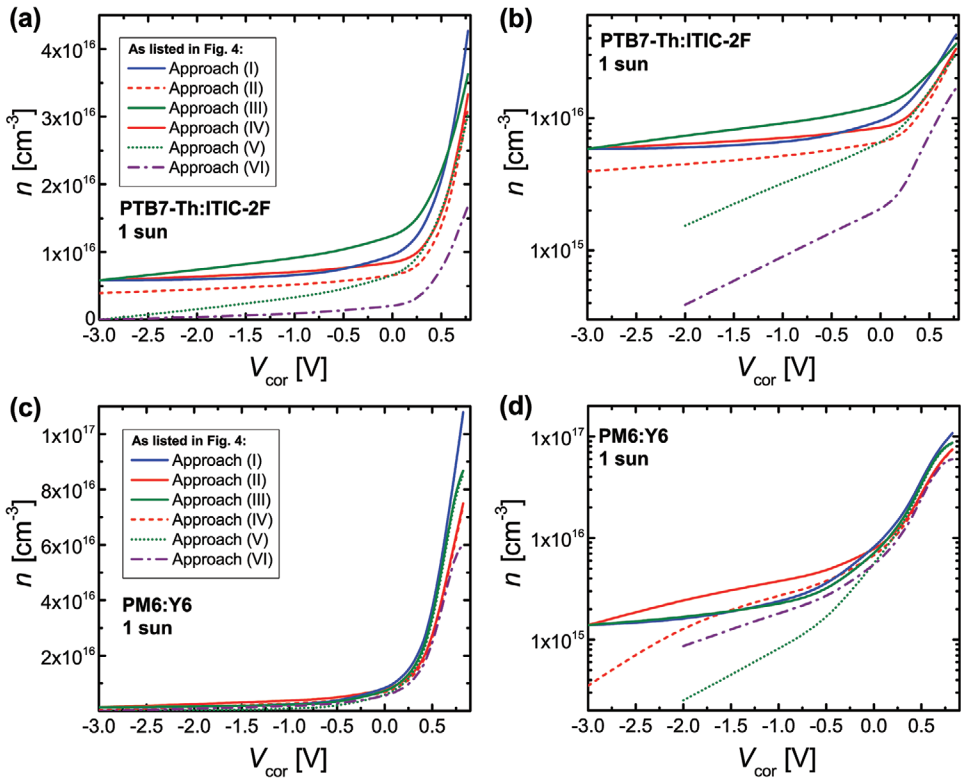

Figure 5. Total charge carrier densities *n* calculated via all relevant methods (I–VI) for a,b) the PTB7-Th:ITIC-2F solar cells and c,d) the PM6:Y6 solar cells.

This approach allows taking into account the voltage-dependent width of the depletion region W independently under illumination and in the dark, as opposite to approach (III), avoiding possible light and light-induced elevated temperature effects on the profile of unintentionally uncompensated donor or acceptor centers in the active layer.

In total, these six relevant methods to obtain the charge carrier density n are listed in Figure 4, where the first three (I–III) have already been used several times in past stu dies.[14,17–20,27,31,32] The other three methods (IV–VI) are introduced to address the shortcomings mentioned earlier. The different total charge carrier densities n resulting from these methods for the investigated PTB7-Th:ITIC-2F and the PM6:Y6 solar cells are compared in **Figure 5**.

At first glance, the variations caused by the different methods to calculate n_{sat} seem to be negligible, if compared to the different approaches for the excess charge carrier density n_{exc}, especially since the saturated charge carrier density n_{sat} tends to linearly change n and is more than one order of magnitude smaller than the highest determined charge carrier density n_{max}, which is found at high forward biases (cf. Tables S3 and S4, Supporting Information). This is especially the case for the PM6:Y6 solar cells, where the curves for (II) and (IV) as well as for (III) and (V) are virtually identical. However, the variations in n_{sat} should not be ignored, specifically if the focus of the analysis lies on the device properties at low or negative biases and/or if the studied devices exhibit an impaired charge extraction. The variations observed for the excess charge carrier density n_{exc} are more pronounced, since they result in different absolute values of n as well as in a different shape of the curves.

2.3. Influence of Varying Charge Carrier Density on Further Analyses

To probe the influence that the differently calculated total charge carrier densities n have on subsequent investigations, we can repeatedly perform the quantitative analysis of the nongeminate recombination dynamics that was introduced in ref. [18] and is summarized again in, cf., Equations (S7)–(S10) in the Supporting Information, taking into account the variations of n that we have discussed previously. This type of analysis is based on the assumption that it is possible to describe the current density lost due to nongeminate recombination, i.e., the recombination current density that we have defined above ($J_{rec} = J_{ph,sat} - J_{ph}$), with the help of the voltage-dependent charge carrier density n. Other known factors such as the charge carrier mobility $\mu_{n/p}$ and dielectric constant ε_r are required as well, and the reduction factor ξ, the density of traps in the bulk N_{tb} and the density of surface traps N_{ts}, which are important to quantify the nongeminate recombination dynamics, act as fitting parameters.[18,20] The fits of the PTB7-Th:ITIC-2F and PM6:Y6 solar cells are depicted in Figures S5 and S6 (Supporting Information). The expected difference of the aforementioned fitting parameters (ξ, N_{tb}, N_{ts}) to reconstruct the recombination current density J_{rec} shall act as an estimate of the impact of the aforementioned variations

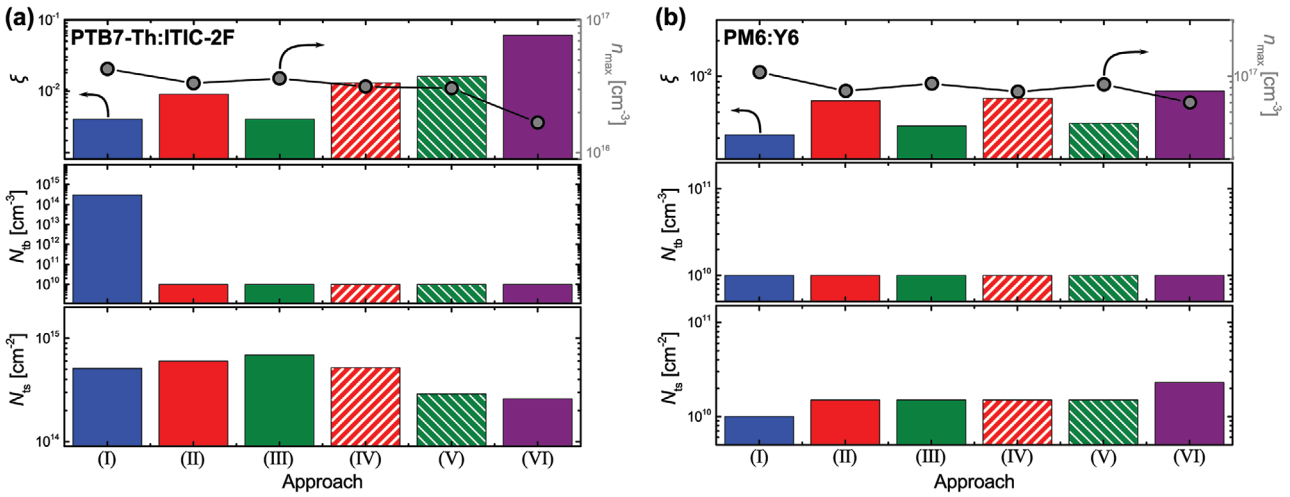

Figure 6. Visual overview of the differences in the fitting parameters (ξ, N_{tb}, N_{ts}) resulting from the variation of the approaches (I–VI) to determine the charge carrier density n as described in Figure 4.

of n resulting from the used method (I–VI) on other analyses, such as the calculation of the effective mobility μ_{eff}, the effective extraction time τ_{ex}, as well as calculations subsequent to the reconstruction of the recombination current density J_{rec}, like the effective charge carrier lifetime τ_{rec}, the recombination coefficients k_{rec}, and the competition factor ($\theta = \tau_{ex}/\tau_{rec}$). Here, we refrain from conducting all of these analyses with the differently obtained charge carrier densities n for the sake of brevity and clarity.

The results for the fitting parameters used to calculate the recombination current density J_{rec} in Figures S5 and S6 (Supporting Information) are summarized in **Figure 6**, while the exact values are listed in Tables S3 and S4 (Supporting Information). The adj. R^2 values may act as a figure of merit for the quality of how the fits compare to the experimentally determined values of J_{rec} that were obtained from the J–V curves. Several different trends can be observed. Most notably, there is an inverse correlation between the charge carrier density at high forward biases n_{max} and the reduction factor ξ. This can be expected, as a higher charge carrier density n in comparison to the same recombination current density J_{rec} will ultimately lead to the result that there is a reduced probability of bimolecular recombination, all else being equal. This can be one explanation for discrepancies of the magnitude of bimolecular recombination determined via capacitance spectroscopy specifically when using approach (I) and other, independent techniques, as was observed for several fullerene systems and is still discussed in the case of PM6:Y6 solar cells.[14,19,33]

Additionally, for the PTB7-Th:ITIC-2F solar cells, approach (I) yields several orders of magnitude higher values for the trap density in the bulk N_{tb} than all the other methods. This seems to be a false result, as independent measurements such as light intensity-dependent J–V curves (i.e., the slope of V_{OC} vs ln[I] plots) and transient V_{OC} decay have shown that there is not any sizeable influence of traps in the bulk.[18] This illustrates how the overestimations of the charge carrier density n inherent to approach (I) can yield significantly different results than the other techniques.

When it comes to the trap densities in the bulk or at the surface (N_{tb}, N_{ts}), there seems to be no real difference in the results for the PM6:Y6 solar cells, which should be expected for such a high performing system that exhibited dominant bimolecular recombination in the other, independent measurements.[19] It should be noted that trap densities of $N_{tb} = 10^{10}$ cm^{-3} and $N_{tb} = 10^{10}$ cm^{-2} constitute the lower boundary used in the fits.

These results cannot act as an ultimate evaluation of the investigated methods that were used to calculate the total charge carrier density n, since they are based only on two datasets. However, they can raise awareness for the dependence of fitting parameters such as the reduction factor ξ and the density of bulk traps N_{tb} on the used method to calculate n. As a rule of thumb, the overestimations of the charge carrier density n due to the variable depletion width W should be avoided. Overestimations resulting from n_{sat} such as in approaches (II) and (III) should also be considered, although subsequent analyses will be less impacted, if high performing solar cells are investigated. On the contrary, these overestimations become important, if the scope of the subsequent analyses lies in the reverse bias regime. Depending on whether the HF regime can be resolved properly and whether the determined charge carrier density n will be put into context with the photocurrent density J_{ph} or not, either method (IV), (V), or (VI) should be chosen as viable alternatives.

3. Conclusion

In this case study we have taken a detailed look at several different methods that have recently been employed to determine the total charge carrier density n via capacitance spectroscopy measurements. Overestimations related to the calculation of the saturated charge carrier density n_{sat} have been revealed, which—to the best of our knowledge—have yet not been discussed anywhere else. Alternative strategies to mitigate these overestimations have been proposed and important parameters for the nongeminate recombination dynamics were quantified

and compared with each other for the dataset obtained from PTB7-Th:ITIC-2F and PM6:Y6 solar cells as a way to assess the influence that varying values of the total charge carrier density n have on these parameters. In essence, the results for bimolecular recombination (reduction factor ξ) are mostly affected by the choice of the approach to calculate the excess charge carrier density n_{exc}. Therefore, great care has to be taken to avoid overestimations of the charge carrier density n due to the variable depletion width W. In contrast, the parameters related to trap-assisted recombination in the bulk and at the surface (bulk trap density N_{tb}; surface trap density N_{ts}) showed mostly only a minor dependence on the chosen approaches to calculate either n_{exc} or n_{sat}. In the future, the results and trends discussed in the scope of this article may act as a guideline and as a starting point for researchers wishing to obtain accurate values for the charge carrier density via capacitance spectroscopy.

Supporting Information

Supporting Information is available from the Wiley Online Library or from the author.

Acknowledgements

J.V. acknowledges funding by the Alexander-von-Humboldt Stiftung.
Open access funding enabled and organized by Projekt DEAL.

Conflict of Interest

The authors declare no conflict of interest.

Keywords

bulk-heterojunction solar cells, capacitance spectroscopy, charge carrier density, impedance spectroscopy, organic photovoltaics

Received: May 20, 2020
Revised: August 5, 2020
Published online: September 11, 2020

[1] B. R. Sutherland, E. H. Sargent, *Nat. Photonics* **2016**, *10*, 295.
[2] J. Vollbrecht, S. Blazy, P. Dierks, S. Peurifoy, H. Bock, H. Kitzerow, *ChemPhysChem* **2017**, *18*, 2024.
[3] H. Sirringhaus, *Adv. Mater.* **2014**, *26*, 1319.
[4] J. Vollbrecht, P. Oechsle, A. Stepen, F. Hoffmann, J. Paradies, T. Meyers, U. Hilleringmann, J. Schmidtke, H. Kitzerow, *Org. Electron.* **2018**, *61*, 266.
[5] A. T. Lill, A. F. Eftaiha, J. Huang, H. Yang, M. Seifrid, M. Wang, G. C. Bazan, T.-Q. Nguyen, *ACS Appl. Mater. Interfaces* **2019**, *11*, 15821.
[6] Y. Rong, Y. Hu, A. Mei, H. Tan, M. I. Saidaminov, S. Il Seok, M. D. McGehee, E. H. Sargent, H. Han, *Science* **2018**, *361*, eaat8235.
[7] Y. Cui, H. Yao, J. Zhang, T. Zhang, Y. Wang, L. Hong, K. Xian, B. Xu, S. Zhang, J. Peng, Z. Wei, F. Gao, J. Hou, *Nat. Commun.* **2019**, *10*, 2515.
[8] J. Huang, A. Karki, V. V. Brus, Y. Hu, H. Phan, A. T. Lill, M. Wang, G. C. Bazan, T.-Q. Nguyen, *Adv. Mater.* **2018**, *30*, 1804794.
[9] J. Lee, S.-J. Ko, H. Lee, J. Huang, Z. Zhu, M. Seifrid, J. Vollbrecht, V. V. Brus, A. Karki, H. Wang, K. Cho, T.-Q. Nguyen, G. C. Bazan, *ACS Energy Lett.* **2019**, *4*, 1401.
[10] J. Huang, J. Lee, J. Vollbrecht, V. V. Brus, A. L. Dixon, D. X. Cao, Z. Zhu, Z. Du, H. Wang, K. Cho, G. C. Bazan, T.-Q. Nguyen, *Adv. Mater.* **2020**, *32*, 1906027.
[11] E. Cantatore, *Applications of Organic and Printed Electronics*, Springer, Berlin **2013**.
[12] L. J. A. Koster, V. D. Mihailetchi, R. Ramaker, P. W. M. Blom, *Appl. Phys. Lett.* **2005**, *86*, 123509.
[13] C. M. Proctor, T.-Q. Nguyen, *Appl. Phys. Lett.* **2015**, *106*, 083301.
[14] M. C. Heiber, T. Okubo, S.-J. Ko, B. R. Luginbuhl, N. A. Ran, M. Wang, H. Wang, M. A. Uddin, H. Y. Woo, G. C. Bazan, T.-Q. Nguyen, *Energy Environ. Sci.* **2018**, *11*, 3019.
[15] T. M. Clarke, C. Lungenschmied, J. Peet, N. Drolet, A. J. Mozer, *Adv. Energy Mater.* **2015**, *5*, 1401345.
[16] G.-J. A. H. Wetzelaer, N. J. Van der Kaap, L. J. A. Koster, P. W. M. Blom, *Adv. Energy Mater.* **2013**, *3*, 1130.
[17] C. M. Proctor, C. Kim, D. Neher, T.-Q. Nguyen, *Adv. Funct. Mater.* **2013**, *23*, 3584.
[18] J. Vollbrecht, V. V. Brus, S.-J. Ko, J. Lee, A. Karki, D. X.i Cao, K. Cho, G. C. Bazan, T.-Q. Nguyen, *Adv. Energy Mater.* **2019**, *9*, 1901438.
[19] A. Karki, J. Vollbrecht, A. L. Dixon, N. Schopp, M. Schrock, G. N. Manjunatha Reddy, T.-Q. Nguyen, *Adv. Mater.* **2019**, *31*, 1903868.
[20] V. V. Brus, C. M. Proctor, N. A. Ran, T.-Q. Nguyen, *Adv. Energy Mater.* **2016**, *6*, 1502250.
[21] G. Garcia-Belmonte, A. Guerrero, J. Bisquert, *J. Phys. Chem. Lett.* **2013**, *4*, 877.
[22] K. Nakano, Y. Chen, K. Tajima, *AIP Adv.* **2019**, *9*, 125205.
[23] V. V. Brus, *Semicond. Sci. Technol.* **2012**, *27*, 035024.
[24] J. Vollbrecht, C. Wiebeler, H. Bock, S. Schumacher, H.-S. Kitzerow, *J. Phys. Chem. C* **2019**, *123*, 4483.
[25] M. P. Hughes, K. D. Rosenthal, N. A. Ran, M. Seifrid, G. C. Bazan, T.-Q. Nguyen, *Adv. Funct. Mater.* **2018**, *28*, 1801542.
[26] P. P. Boix, A. Guerrero, L. F. Marchesi, G. Garcia-Belmonte, J. Bisquert, *Adv. Energy Mater.* **2011**, *1*, 1073.
[27] G. Garcia-Belmonte, P. P. Boix, J. Bisquert, M. Sessolo, H. J. Bolink, *Sol. Energy Mater. Sol. Cells* **2010**, *94*, 366.
[28] S. M. Sze, K. K. Ng, *Physics of Semiconductor Devices*, Wiley Online Library **2006**.
[29] A. Karki, G.-J. A. H. Wetzelaer, G. N. M. Reddy, V. Nádaždy, M. Seifrid, F. Schauer, G. C. Bazan, B. F. Chmelka, P. W. M. Blom, T.-Q. Nguyen, *Adv. Funct. Mater.* **2019**, *29*, 1901109.
[30] I. Lange, J. C. Blakesley, J. Frisch, A. Vollmer, N. Koch, D. Neher, *Phys. Rev. Lett.* **2011**, *106*, 216402.
[31] I. Zonno, H. Zayani, M. Grzeslo, B. Krogmeier, T. Kirchartz, *Phys. Rev. Appl.* **2019**, *11*, 054024.
[32] L.-W. Feng, J. Chen, S. Mukherjee, V. K. Sangwan, W. Huang, Y. Chen, D. Zheng, J. W. Strzalka, G. Wang, M. C. Hersam, D. DeLongchamp, A. Facchetti, T. J. Tobin, *ACS Energy Lett.* **2020**, *5*, 1780.
[33] L. Perdigón-Toro, H. Zhang, A. Markina, J. Yuan, S. M. Hosseini, C. M. Wolff, G. Zuo, M. Stolterfoht, Y. Zou, F. Gao, D. Andrienko, S. Shoaee, D. Neher, *Adv. Mater.* **2020**, *32*, 1906763.